Statistical Comparisons of Observed and ECMWF Modeled Open Ocean Surface Drag

H. Bonekamp,* G. J. Komen, and A. Sterl

Oceanographic Research Division, Royal Netherlands Meteorological Institute, De Bilt, Netherlands

P. A. E. M. Janssen

European Centre for Medium-Range Weather Forecasts, Reading, United Kingdom

P. K. Taylor and M. J. Yelland

James Rennell Division, Southhampton Oceanography Centre, Southhampton, United Kingdom

ABSTRACT

The surface-drag coefficients of two versions of the ECMWF's atmosphere–wave model are compared with those of uncoupled model versions and with those of inertial-dissipation measurements in the open ocean made by the RRS *Discovery*. It is found that the mean drag resulting from the latest coupled version is on average equal to that of the uncoupled version. However, both have a positive bias when compared with the RRS *Discovery* observations. This bias is discussed, also in the light of other observational open ocean data. In the second part of the paper, bulk parameterizations with and without parameters of collocated sea-state data are validated against the *Discovery* observations. Using published estimates of the error in friction velocity and the neutral 10-m winds, all bulk parameterizations score low on goodness-of-fit tests. The lowest scores are obtained for the constant Charnock parameter case, whereas the highest scores are obtained for a wave-age-dependent parameterization. On–off experiments are made for the corrections to the inertial-dissipation data that have been proposed in previous studies. These corrections concern the measurement height and the direct wave-induced turbulence in the lower atmosphere. The first correction results in a slightly better agreement, but the second reduces the goodness-of-fit of the bulk parameterizations.

1. Introduction

The momentum exchange at the atmosphere–ocean interface is a key quantity in analyses and predictions of the sea state, weather, and climate (see, e.g., WGASF 2000). Therefore, accurate measurements and model parameterizations of the wind stress are essential for an increasing reliability of these analyses and predictions.

Quantitatively, the momentum exchange is expressed in terms of the wind stress (e.g., Stull 1988; Garrat 1992). The magnitude of the kinematic surface wind stress is given by

$$\tau = u_*^2 = [(\overline{u'w'})^2 + (\overline{v'w'})^2]^{1/2}, \qquad (1)$$

where u', v', and w' are the turbulent fluctuations of the 3D components of the near-surface wind. The ov-

erbar denotes the averaging over a suitable time period (approximately 20 min). Equation (1) is the definition of the friction velocity u_*, which is the scale parameter for the turbulent motions in the shear flow.

In general, it is not feasible to model the evolution of the turbulent quantities of equation (1) explicitly. Therefore, τ is parameterized in terms of surface and near-surface variables (first-order turbulent closure). The wind stress strongly depends on the mean near-surface wind u. This dependence is expressed by the bulk transfer formula

$$\tau = u_*^2 = C_d u^2, \qquad (2)$$

where C_d is the drag coefficient. The theoretical basis for the parameterization of C_d is the Monin–Obukhov similarity theory, which was originally developed for wind stress over land (e.g., Monin and Obukhov 1954; Stull 1988; Garrat 1992). This theory relates the vertical profile of the wind shear to the aerodynamical roughness of the surface and the stability of the atmosphere. The profile is given by (e.g., Garrat 1992)

$$u(z) = \frac{u_*}{\kappa}\left[\ln\left(\frac{z}{z_0}\right) - \psi_m\left(\frac{z}{L}\right)\right], \qquad (3)$$

---

* Current affiliation: Civil Engineering and Geosciences, Delft University of Technology, Delft, Netherlands.

Corresponding author address: Dr. H. Bonekamp, Oceanographic Research Division, Royal Netherlands Research Institute (KNMI), Box 201, AE De Bilt NL-3730, Netherlands.
E-mail: j.g.bonekamp@ct.tudelft.nl

where κ is the von Kármán constant (0.40), z the reference height, z_0 the aerodynamical surface roughness length, L the Obukhov stability length, and $\psi_m()$ the stability correction function. The Obukhov stability length is the height at which the shear production equals the buoyancy production (destruction) of turbulent kinetic energy (TKE). Depending on L, the stability correction $\psi_m(z/L)$ is, respectively, positive, zero, or negative for unstable, neutral, or stable atmospheric stratifications.

Over land, the aerodynamical roughness of the surface is in general static, because a one-to-one correspondence can be made between z_0 and the typical roughness elements for the different vegetations, rocks, or land use, etc. (e.g., Stull 1988). However, over the ocean the aerodynamical roughness is dynamically determined by the presence of time-varying gravity waves, capillary waves, white caps, etc. The oceanic aerodynamical roughness length z_0 has the following functional form (Smith 1988)

$$z_0 = 0.11 \nu/u_* + \alpha u_*^2/g. \qquad (4)$$

The first term is the roughness length for smooth surfaces, where the drag is produced by viscous friction (ν is the molecular viscosity of air). This term is significant for the light wind cases ($u_{10n} < 5$ m s^{-1}). The second term is the roughness length for rough flow conditions, where the drag is brought about by turbulence. This term dominates z_0 for wind speeds over 5 m s^{-1}. Its functional form has been proposed by Charnock (1955) assuming a dominant role of gravity waves for the momentum transfer. The parameter α is the dimensionless aerodynamical surface roughness or Charnock parameter.

Over the open ocean the atmosphere is usually neutral or slightly unstable. For moderate to strong winds (6–25 m s^{-1}) focused on in this paper the stability corrections are very small. This makes it meaningful to write

$$C_d = C_{dzn}(1 + \delta_s) \qquad (5)$$

with $\delta_s \ll 1$. The so-called neutral drag coefficient

$$C_{dzn} = \kappa^2/\ln^2[z/z_0] \qquad (6)$$

in turn defines the neutral wind speed

$$u_{zn} = u_*/\sqrt{C_{dzn}}. \qquad (7)$$

These equations show that z_0 is the quantity of central interest. Therefore, we will focus on a comparison of observed and modeled values of z_0.

Equations (6) and (7) are usually applied at 10-m height. In the rest of this paper we will use the notation C_{d10n} and u_{10n}. These quantities can be interpreted as the drag coefficient and the 10-m wind that would be obtained for the given roughness but under neutral conditions.

The literature on ocean drag coefficients and Charnock parameters is very extensive. Most studies have confirmed an increase of C_{d10n} with u for wind speeds

larger than approximately 5 m s^{-1}. However, a subject of debate is the parameterization of the effects of sea-state variability. Important questions are 1) Can the adjustment of the aerodynamical roughness be considered as (quasi-) instantaneous to u or should the drag relation (6) include explicit parameters of the sea state? 2) If any, which sea-state parameters should be included? The literature on this issue has been reviewed by, for example, Donelan (1990), hereafter (D90) and Komen et al. (1998). Komen et al. (1998) have stressed that the range of sea-state conditions is not easily described by a single parameter (such as wave age). They concluded that ideal stress measurements would include the full two-dimensional spectrum of the surface waves.

In the spring of 1998, the European Centre for Medium-Range Weather Forecasts (ECMWF) introduced the coupling of its atmospheric forecast model to a wave model to include sea-state information in the model determination of surface winds and wind stress. The coupling follows the ideas of Janssen (1989, 1991) and the wave model used is the WAM (Komen et al. 1994). In particular, the Charnock parameter, which was previously used as a constant with a value of 0.018, was made dependent on the 2D spectrum of the modeled surface waves. The coupling has a beneficial impact on the ECMWF's short and medium-range forecasts (e.g., Janssen et al. 1999). In addition, Janssen and Viterbo (1996) made an extensive study regarding the impact of the coupling on the wind and wave climate. With new versions of the ECMWF model, validation of the surface fluxes remains an important issue.

To support climate variability studies and seasonal forecasting, the ECMWF assimilates archived observations in lengthy reanalyses of the atmosphere. A 15-yr reanalyses from 1979 and to 1994 (ECMWF Re-Analysis 15, hereafter ERA15) has been successfully completed (Gibson et al. 1997). This reanalysis has used the uncoupled ECMWF model, that is, $\alpha = 0.018$. A new reanalysis will be generated for the period 1958–98 (ERA40) with a coupled wind–wave model (Uppala et al. 2000). In this study, we will compare the mean drag coefficients from ERA15 and ERA40 test experiments.

Wind stress or u_* can be measured and several recent experiments have produced valuable new sets of observed wind stress and other near-surface data. Examples of such experiments include the Southern Ocean Waves Experiments (SOWEX; Banner et al. 1999), the Fronts and Atlantic Storm Tracks Experiment (FASTEX; e.g., Hare et al. 1999; Eymard et al. 1999), and the wind stress observations obtained from the Royal Research Ship *Discovery* (Yelland and Taylor 1996). These and other studies have confirmed the increase of C_{d10n} with the mean wind speed, which is often expressed as

$$C_{d10n} = a + bu_{10n}, \qquad a, b > 0. \qquad (8)$$

However, empirical studies differ with respect to lo-

cation, month, length, mean geophysical conditions, measurement accuracy, and quality of wave measurements (if any). As a result, there is a lot of scatter in the drag coefficients suggested by the different experiments (e.g., Banner et al. 1999, their Fig. 1).

Instrumentation, measurement technique, and restricted sampling lengths introduce systematic and random errors in observed wind stresses. In every experiment these errors obscure the influence of the varying geophysical conditions. Systematic errors caused by external factors (flow distortion, measurement height) or theoretical shortcomings are sometimes compensated for. However, corrections are often approximations with new errors. Some studies have made an assessment of the random errors on the basis of statistical analyses (e.g., Sreenivasan et al. 1978) or on the basis of intercomparisons and sensitivity studies (Yelland et al. 1994; Yelland 1997). These studies demonstrate that the size of random errors is comparable to the variability observed for a given range of the mean wind speed. This makes the identification of geophysical variability (e.g., induced by the varying sea state) a difficult task.

The most extensive dataset of wind stress observations is the *Discovery* dataset (Yelland and Taylor 1996). A few thousands of wind and wind stress measurements were gathered during several cruises of the research vessel in the Southern Ocean. The measurement technique was the inertial-dissipation (ID) method. Yelland et al. (1998) have corrected the *Discovery* data for flow distortion by the ship. Others have suggested additional corrections. In particular, Janssen (1999, hereafter J99) has suggested that the ID method neglects fluctuations in the balance of turbulent kinetic energy caused by the surface waves. The result of this neglect may be an underestimation of the wind stress, especially for large wind speeds. J99 has proposed a correction to the ID method based on a simple spectral form for the wind waves. This correction for ocean wave effects is still a matter of debate (Taylor and Yelland 2001; Janssen 2001). Finally, D90 suggested that observed wind stresses need a correction for large (>10 m) measurement heights.

In this paper, we report our work on the validation of open ocean wind stress parameterizations in the successive versions of ECMWF's atmospheric model. Our focus is on wind stress at the open ocean and on the wind stress product from the ECMWF reanalyses. In particular, we verify the following two requirements (in decreasing order of importance). 1) Model wind stress should not be largely biased with respect to observed wind stress. 2) The parameterization should give a fair description of observed geophysical variability. We use the *Discovery* dataset as the main observational dataset. The length of this set is very relevant for validation studies; it enables a more rigorous statistical assessment (see also, e.g., Janssen 1997) of the mean and deviations from the mean for various wind speed ranges. Wind stress measurements of other open ocean experiments

are used as a background check. We also consider the combined impact of the measurement height (D90) and the J99 corrections on the comparison.

In addition, and related to the assessment of ECMWF's drag coefficients, we revisit the question whether the *Discovery* data support sea-state dependent bulk parameterizations. On the basis of a rough estimate of the peak velocity of the waves, Yelland et al. (1998) have concluded that a wave-age dependent (e.g., Smith et al. 1992) parameterization of the wind stress is redundant for the *Discovery* data. However, they did not compare the goodness-of-fit of this parameterization with other parameterizations. In this paper, we have made a statistical assessment of a hierarchy of parameterizations ranging from the constant Charnock parameter case to a parameterization that depends on the wave-induced stress (Janssen 1991). We have used the estimates of Yelland (1997) for the random measurement errors of the *Discovery* data. Collocated wave data required for the sea-state-dependent parameterizations are obtained from the uncoupled WAM model run as described in J99. In this part of the study, only winds stronger than 8 m s^{-1} are used to diminish the effects of atmospheric (in)stability and to enhance the relative importance of wind waves in the total wave spectrum. An attempt is made to answer the question to what extent the variance could be explained by experimental noise or by geophysical variance. Again we consider the combined impact of the measurement height and the J99 corrections.

The outline of the paper is as follows. Section 2 contains a description of the ECMWF parameterization of the wind stress. The description of the surface stress observations by the RRS *Discovery* follows in section 3. The direct comparison of drag coefficients from the different ECMWF model versions with observations is given in section 4. The statistical assessment of the hierarchy of parameterizations for the *Discovery* data is presented in section 5. Finally, we discuss and summarize our results in section 6.

2. ECMWF wind stress data

In the ECMWF atmospheric model, wind stress is calculated from surface quantities and parameters at the lowest model level z_l, which is at about 24 m for both reanalyses. The calculations are based on the Monin–Obukhov similarity theory. The drag coefficient is determined using the vertical profile of Eq. (3) and a roughness length given by Eq. (4). The exact formulation can be found in section 3.4 of ECMWF (1998).

The modeling of the aerodynamical roughness length for rough flow [second term of Eq. (4)] has been the subject of modification in the recent model versions. Originally, in the uncoupled model versions, a constant value of $\alpha = 0.018$ was used. From June 1998 onward, α is determined from the surface wave spectrum modeled by the WAM wave model (Komen et al. 1994)

TABLE 1. ECMWF experiments with different parameterization of the wind stress. See text for explanation. The spectral triangular grids T106 and T159 are roughly equivalent to regular $1.1° \times 1.1°$ and $0.75° \times 0.75°$ longitude–latitude grids, respectively.

Experiment	Coupling	Hor. reso-lution	Period
ERA15	—	T106	Jan 1979–Feb 1994
AVOT	—	T159	May 1986–Jun 1989
AW5D	Old WAM	T159	May 1987–Oct 1987
0147	New WAM	T159	Jul 1987–Nov 1987
OLERA15	Offline WAM	T106	Jan 1979–Feb 1994

coupled to the atmospheric model. More precisely, the Charnock parameter is determined from the ratio of the wave-induced stress τ_w and the total momentum flux as

$$\alpha = \frac{\hat{\alpha}}{\sqrt{1 - |\boldsymbol{\tau}_w|/u_*^2}} \qquad (9)$$

(Janssen 1991). The parameter $\hat{\alpha}$ is set to 0.010. The wave-induced stress τ_w is given by the following integral

$$\boldsymbol{\tau}_w = \frac{2\pi g}{\epsilon} \iint df \, d\theta \gamma N \mathbf{k}, \qquad (10)$$

where γ is the wave growth rate, ϵ the air–water density ratio, N the action density spectrum, and $\mathbf{k}$ the wave-number. The dynamical evolution of the wave spectrum is calculated in the WAM model over a finite frequency range. Bidlot et al. (1999) have reported a modification to the high-frequency cutoff value f_c of this range. The main reason was a more realistic simulation of the mean square slope. In the old version f_c is set to the maximum of 2.5 times the mean frequency and 4 times the Pierson–Moskowitz frequency (e.g., Pierson and Moskowitz 1964). The latter alternative was originally introduced to include the wind sea in the frequency range for cases with both swell and wind sea. In the new version (here called ''coupled new'') the alternative is canceled, setting f_c to 2.5 times the mean frequency. The modification has consequences for the wind stress, as will be shown in section 4.

Several experiments with different coupled model configurations have been performed at ECMWF. The experiments considered in this paper are summarized in Table 1. Both ERA15 and AVOT used $\alpha = 0.018$. Differences between the two runs were the period and horizontal resolution. AW5D and 0147 are experiments with the old and the new version of the WAM model, respectively. The 0147 configuration is suggested to be used for ERA40. Finally, in the OLERA15 experiment, the drag coefficients are calculated from the hindcast run of Sterl et al. (1998). In this run the WAM model is forced with the ERA15 surface winds. The drag coefficients are calculated on the basis of Eq. (9). In this case, the wind stresses do not feed back on the dynamic evolution of the atmosphere.

For all the test experiments, ECMWF has archived the horizontal wind fields at the height of 10 m. Here we use the 10-m wind fields of the daily analysis at 1200 UTC. In addition, for the coupled models the two-dimensional fields of the Charnock parameter α are stored. Neutral drag coefficients are calculated from Eq. (6) and the second term of (4), which are solved implicitly for u_* using a Newton iteration method and approximating $u_*^2 = C_d u_{10}^2$ by $u_*^2 = C_{d10n} u_{10}^2$. In this way the effects of stability (Eq. 3) and the viscous roughness term [first term of Eq. (4)] are neglected. This is justified for moderate to strong winds (6–25 m s^{-1}) and for the slightly unstable condition of the open ocean. Differences in terms of C_{d10n} and $C_d(z_l = 10$ m) are less than 2%.

In this way we have prepared a standard dataset for each of the runs of Table 1, containing u_{10n}, z_0, α, and C_{d10n}. These will be used in section 4 for the comparison with observations.

3. Observational data

The drag coefficient measurements of the RRS *Discovery* (Yelland and Taylor 1996) are used for a comparison with the drag parameterizations of the ECMWF model. The RRS *Discovery* has made several cruises in the Southern Ocean in the period from December 1992 to April 1993. The friction velocity u_* was measured with the inertial-dissipation method. Yelland et al. (1998) applied a correction for the flow distortion by the ship and used the imbalance term as described in Yelland and Taylor (1996). In a subsequent study, Taylor and Yelland (2000) concluded that the (empirically determined) Yelland and Taylor (1996) imbalance can be explained by the random errors in the u_* determination. They reprocessed the Yelland et al. (1998) data without an imbalance term, but with the Henjes et al. (1999) correction for the pulse averaging and with an alternative method for the iterative calculations. In this study we use the Taylor and Yelland (2000) reprocessed *Discovery* data (Disc2000) as the basic observational dataset for the comparisons with the ECMWF model stress data.

Observational data from other open ocean experiments are also available for comparison. Table 2 lists the measurement experiments considered in this paper. Smith (1980) and Eymard et al. (1999) [Couplage avec l'atmosphère en Conditions Hivernales (CATCH)/FASTEX] applied only the eddy correlation (EC) method and the ID method, respectively, whereas in the experiments of Banner et al. (1999) (SOWEX) and Hare et al. (1999) (FASTEX) both the EC and ID were used. Finally, from the Tropical Ocean Global Atmosphere Comprehensive Ocean–Atmosphere Response Experiment (TOGA COARE) (Fairall et al. 1996) only the ID measurements as compiled by Zeng et al. (1998) are used.

In both the EC and ID method, the wind stress (or u_*) is calculated from the fluctuations in wind mea-

TABLE 2. Measurement technique of the different open ocean experiments. The eddy correlation and inertial dissipation method are denoted by EC and ID, respectively. The last column indicates whether a flow distortion correction (FCD) is applied.

Experiment	Method	FDC
Banner et al. (1999) (SOWEX)	EC and ID	− (EC) − (ID)
Eymard et al. (1999) (CATCH/FASTEX)	ID	−
Zeng et al. (1998) (TOGA COARE)	ID	−
Hare et al. (1999) (FASTEX)	EC and ID	+ (EC)* + (ID)
Smith (1980)	EC	−
Taylor and Yelland (2000)	ID	+

surements. These calculations cannot be made without random sampling errors due to the turbulence and instrumental shortcomings. For the eddy correlation method Sreenivasan et al. (1978) argued that the sampling errors in u_* can be considered as normally distributed and they give the following estimate for their relative magnitude,

$$\epsilon_{u_*} = \frac{\sigma_{u_*}}{u_*} = \sqrt{\frac{7.5 z_{obs}}{u\Omega}}, \tag{11}$$

where Ω is the duration of the sampling record and z_{obs} the measurement height.

Yelland et al. (1994) have made an intercomparison of u_* observations from setups with different anemometers. The spread found is an approximation of the instrumentation errors in their ID method. In addition, Yelland (1997) has made several sensitivity checks and concluded that good estimates for the combined instrumentation and sampling error for u_* and u_{10n} are

$$\epsilon_{u_*} = \frac{\sigma_{u_*}}{u_*} = 0.06, \tag{12}$$

$$\epsilon_{u_{10n}} = \frac{\sigma_{u_{10n}}}{u_{10n}} = 0.03. \tag{13}$$

For a duration of the sampling record of 30 min and for $u_{10n} \approx 10 \text{ m s}^{-1}$ the estimates (12) and (11) have the same magnitude, suggesting that the EC and ID method are equally accurate with respect to the sampling errors.

The sampling errors in u_* and u_{10n} have serious consequences for the random errors in the neutral drag coefficient C_{d10n} and the Charnock parameter α. Assuming that the random errors for u_* and u_{10n} are independent, the corresponding relative error for C_{d10n} is in first order approximated by

$$\epsilon_{C_{d10n}} \approx 2\sqrt{\epsilon_{u_*}^2 + \epsilon_u^2} = 0.134. \tag{14}$$

This value exceeds $2\epsilon_{u_*}$ by only 1.4%. Hence, the sampling error in C_{d10n} is dominated by the sampling error of u_* and, consequently, the distribution of the C_{d10n} is fairly symmetric. In addition, the exponential dependence of the Charnock parameter α on u_* and u_{10n} has serious consequences for the size and distribution of random errors of α. Neglecting the viscous surface roughness, α is computed from Eqs. (4) and (6) as

$$\alpha = \frac{10g}{u_*^2} \exp\left(-\frac{\kappa u_{10n}}{u_*}\right). \tag{15}$$

The values for the *Discovery* data are shown in Fig. 1. The plot shows a large scatter with a highly skewed distribution in every wind speed range. The largest scatter is for the lower wind speeds. Neglecting the sampling errors in u_{10n}, the conditional probability distribution function (PDF) of α for a fixed value of u_{10n} can be inferred from (15) using the normal distribution of the u_*. This conditional PDF is given by

$$f_\alpha(\alpha \,|\, u_{10n}) = \frac{u_*^2}{\alpha[\kappa u_{10n} - 2u_*]}$$

$$\times \left\{ \frac{1}{\sqrt{2\pi}\epsilon u_*^e} \exp\left[\frac{-(u_* - u_*^e)^2}{2\epsilon^2(u_*^e)^2}\right] \right\}, \tag{16}$$

where u_*^e and ϵu_*^e are the expected value and standard deviation (sampling error) of u_*. In this equation the actual values of u_* must be determined implicitly from α and u_{10n} using (15). The conditional PDF is plotted in Fig. 2 for a fixed wind speed $u_{10n} = 10 \text{ m s}^{-1}$ and different values of ϵ. The value of u_*^e is chosen to be 0.379, which results from Eq. (15) in an expected value of α of 0.018. Figure 2 demonstrates that for larger ϵ the distribution is very skewed. Relative errors in α exceeding 50% are not exceptional. A consequence of the skewness of the distribution (16) is that an averaged α for a fixed wind speed bin as computed, for example, by (Hare et al. 1999, Fig. 5), has a positive bias with respect to the expected (true) value of α due to the observational errors in u_*. Actually, the factor $u_*^2/\alpha[\kappa u_{10n} - 2u_*]$ is neglected. The effect is illustrated in Fig. 3. The overestimation is strongest for lower wind speeds, which confirms the strong scatter in Fig. 1 for this range. The median value of α in the wind speed bin remains unbiased and is therefore a better estimator of the expected α. For the same reason an unweighted least squares fitting to observed α values, as used, for example, by Banner et al. (1999) is questionable with random errors in u_* larger than 3%.

Not only random but also systematic errors may have a serious impact on observed wind stresses. D90 noted that the assumption of a constant stress layer, which is the basis for the logarithmic profile [e.g., Eq. (3)], is valid up to a height of approximately 10 m. Above this
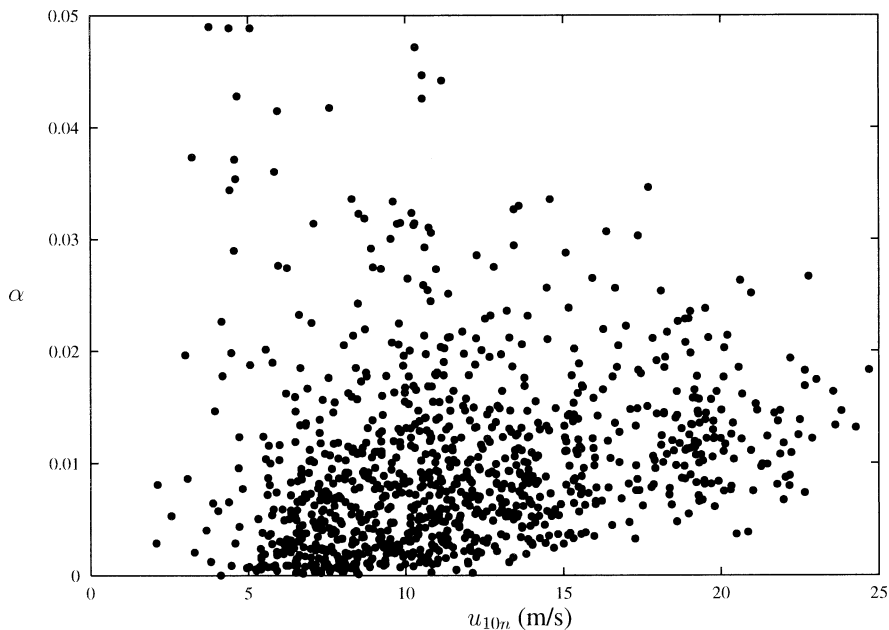
FIG. 1. Charnock parameter α as a function of the wind speed for the *Discovery* data (Taylor and Yelland 2000).

height wind stress may decay with height. Without correction this may result in an underestimation of the stress. He estimated the decay as

$$u_*^2(z) = u_*^2(0)\left[1 - \frac{cf_{coriolis}z}{u_*(0)}\right], \qquad (17)$$

where $c \approx 12$ and $f_{coriolis} = 1.454 \times 10^{-4}$ sin (latitude)

is the Coriolis parameter. For the measurement height (≈ 17.50) and latitude ($\approx 45°S$) of the *Discovery* data, the estimate (17) corresponds to an increase in wind stress of approximately 5% (2%) for moderate (strong) winds. Another correction for wind stress measurements with the ID method has been suggested by J99. The common ID method neglects the effect of surface waves
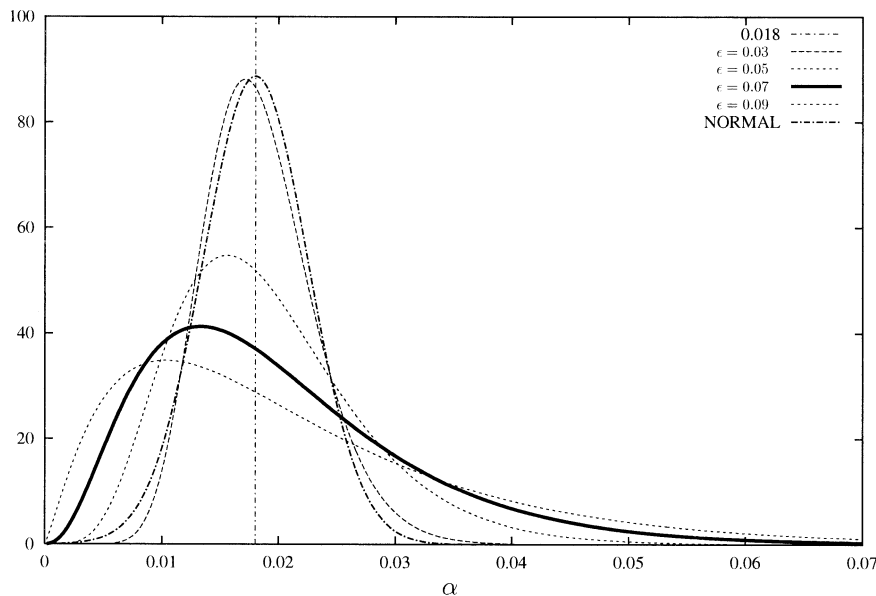
FIG. 2. PDF of the Charnock parameter α at a wind speed of 10 m s^{-1} as a result of errors in the friction velocity u_*. The expected value of α is 0.018. The errors in u_* are assumed to be Gaussian distributed with a relative error, $\epsilon = \sigma_{u_*}/u_*$. Lines are shown for different values of ϵ. As a reference, the dashed–dotted line is a Gaussian distribution for α with a relative error in α of 25%.
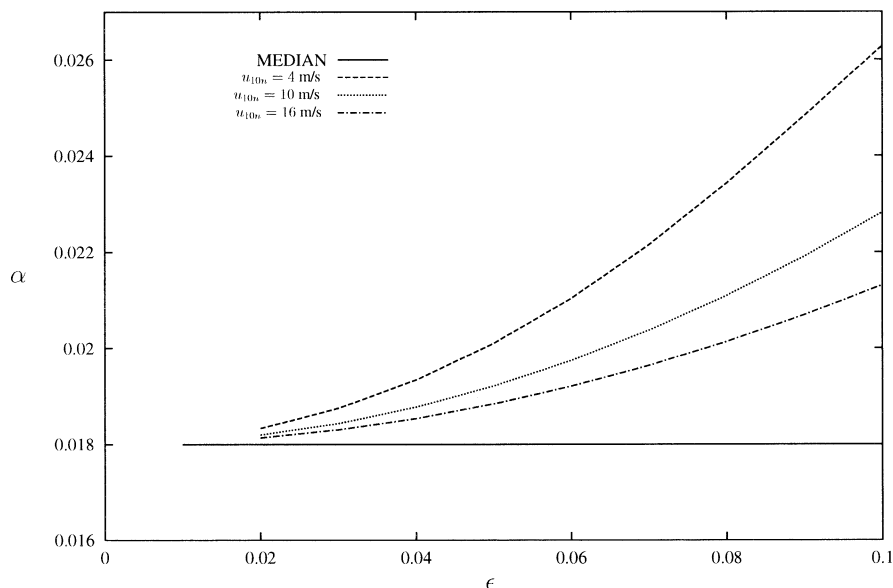
FIG. 3. The median and mean value of the Charnock parameter α as estimators for the expected value ($\alpha = 0.018$) and shown as a function of the relative error in the friction velocity $\epsilon = \sigma_{u_*}/u_*$. The errors in u_* are assumed to be Gaussian distributed. Lines are shown for different values of the wind speed. Clearly, only the median of α is unbiased. The bias in the mean decreases with an increasing wind speed.

on the balance of the turbulent kinetic energy (TKE) in the lower atmospheric boundary layer. This neglect may result in an underestimation of the wind stress. On the basis of a simple model for the surface waves, J99 proposed the correction

$$u_*^{\mathrm{cor}} = u_*^{\mathrm{org}}\left(\frac{1}{1 + I_w^*}\right)^{1/3}, \qquad (18)$$

where I_w^* is an estimation of the nondimensional TKE associated with wave-induced pressure fluctuations. Here u_*^{cor} is larger than u_*^{org} because I_w^* is negative. The strongest effect is for the highest wind speeds (J99, his Fig. 3). The J99 correction does not apply to EC method, because the observed turbulent wind fluctuations [Eq. (1)] must include the wave-induced motions in the atmosphere. In this paper the combined effects of the measurement height (MH) and the J99 correction [where the I_w^* estimate is taken from Janssen (2001)] are studied in additional on-off experiments.

4. Comparison of mean drag coefficients

For all the ECMWF test experiments of Table 1 wind stresses are calculated from the 10-meter wind analyses of 1200 UTC and the Charnock parameter as described in section 2. Data are selected from 65° to 40°S and from 10°W to 90°E. This area overlaps the cruises of the RRS *Discovery*. The selected time period is from 1 August 1987 to 14 August 1987. The calculated drag coefficients are divided into u_{10n} bins of 0.5 m s^{-1}. The resulting curves for the various experiments are plotted

in Fig. 4 together with the mean drag coefficients of the Disc2000 data.

All model-derived C_{d10n}–u_{10n} relations are significantly higher than that of the Disc2000 data. Closest to the observations are the ERA15 and the 0147 (ERA40) model (overestimation of 10%). The 0147 has slightly lower drag coefficients for the wind speed range of 6–12 m s^{-1}. For wind speeds over 12 m s^{-1}, the 0147 drag coefficients are larger. As a result, the slope of the 0147 slope is more consistent with the observations. For the old coupled model (AW5D) the differences with the Disc2000 data are substantially larger (25%), which has also been reported by Bidlot et al. (1999) and Yelland and Taylor (1999). The curve from AVOT is not shown because it nearly overlaps that of ERA15. This suggests that the differences found between the model curves are solely due to the wave coupling and not to the increase in resolution. Finally, the largest difference is obtained for the offline model run (30%–40%). In this run the drag coefficient is directly calculated from the WAM model output by applying Eq. (9) without feedback to the surface wind. Differences between the uncoupled and the offline model have been discussed in detail by Sterl and Bonekamp (2000). They suggested that part of the difference can be explained from the absence of the wave-to-atmosphere feedback, which would enhance the shear, lower the u_{10n} wind speeds, and subsequently, lower the stress.

The difference in the scatter of the Charnock parameter of the old and new coupled model is investigated by sorting the data into two-dimensional bins with the
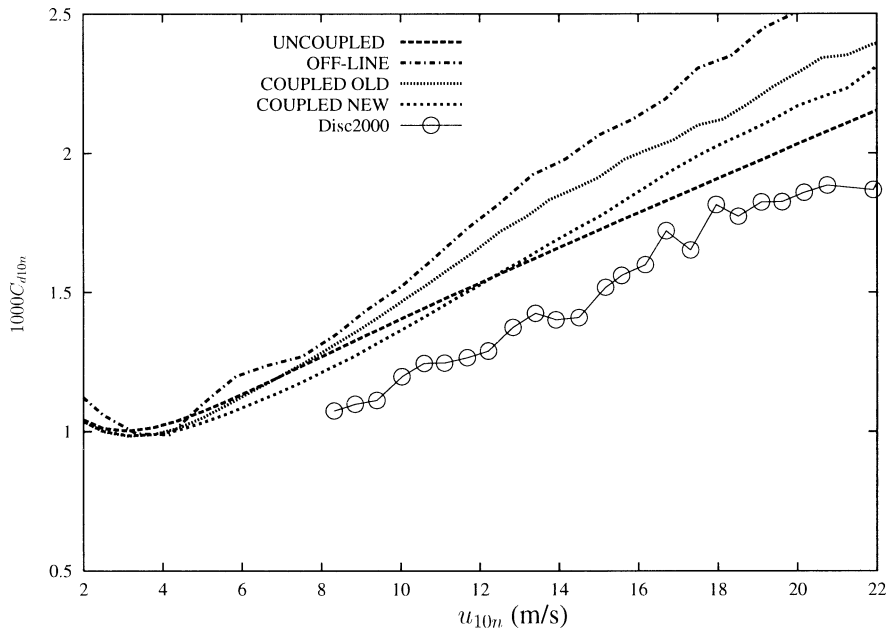
FIG. 4. The mean drag coefficient as a function of wind speed. Five curves are shown. The dashed, dashed–dotted, dotted, and solid line are for the uncoupled model (ERA15), the offline model run (OL-ERA15), the old coupled model (AW5D), and the new coupled model (0147), respectively. The line with open circles is for the *Discovery* data (Taylor and Yelland 2000).

inverse wave age u_*/c_p (c_p is the peak phase velocity of the surface waves) on the x axis and the magnitude of α on the y axis. This is shown in Fig. 5 for all wind speed classes. The gray scales in Fig. 5 give the percentage of the total number of data and indicate the scatter of α. First, from Eq. (9) the model Charnock parameters are bound to be larger than $\hat{\alpha} = 0.01$. This means that the many observed low values (Fig. 2) cannot be modeled. Thus, a large value of $\hat{\alpha}$ is a possible explanation for the model drag coefficients to be higher than those in the Disc2000 dataset. Second, the scatter of the old coupled model is much larger than that of the new coupled model, especially for the older waves. In these cases the alternative cutoff frequency (based on the Pierson–Moskowitz frequency, see section 2) may be active. Third, as a reference the linear relation, $\alpha = 0.5\, u_*/c_p$, (dashed line) is plotted in Figs. 5a and 5b. In the new coupled model, this line is a fair guide for the most likely α's given a fixed wave age. Moreover, the modeled α's are fairly symmetrically distributed around this line, which suggests that, theoretically, a wave-age-dependent Charnock parameter as considered by, for example, Smith et al. (1992) is a good approximation for the sea-state dependency of surface roughness. The goodness of fit of this parameterization is tested for the Disc2000 dataset in section 5. The Charnock parameters of the old coupled model (Fig. 5a) are often much higher than the indicated linear relation, which is a clear explanation for the higher neutral drag coefficients in this case (see Fig. 4).

As pointed out in section 3 the Disc2000 data are

possibly subject to systematic errors, which can be corrected for. The impact of the MH and J99 correction is demonstrated in Fig. 6. The MH correction has a small impact. The absolute correction of C_{d10n} increases only slowly with u_{10n}. However, the impact of the J99 correction is larger for wind speeds above 10 m s^{-1}. The correction increases with u_{10n}. The combined MH and J99 corrections give C_{d10n}'s that are nearly equal to the new coupled model values for the highest wind speeds ($\approx$20 m s^{-1}). For moderate winds only the MH corrections reduces the bias, but a significant overestimation of the model remains.

Finally, to further investigate the bias between the new coupled model and the Disc2000 data a comparison with the neutral surface drag of other open ocean experiments is made. The measurement technique used by the experiments and the application of a flow distortion correction are listed in Table 2. The comparison in terms of median and average Charnock parameters is shown in Fig. 7a. Clearly, as discussed in this section, inaccuracies in the plotted points and curves may be large (10%–40%) due to the large sampling errors and (in many cases) small number of observations. The random uncertainty is illustrated in the bottom panel of Fig. 7. Ninety percent error bars are plotted for the Disc2000 values and those of Banner et al. (1999). The first have the smallest random errors in the median values due to the large number of observations, whereas the latter may have the largest uncertainty due to the small number of observations. The random errors in the median (mean) values of the other experiments may lie in between.

COUPLED OLD

COUPLED NEW
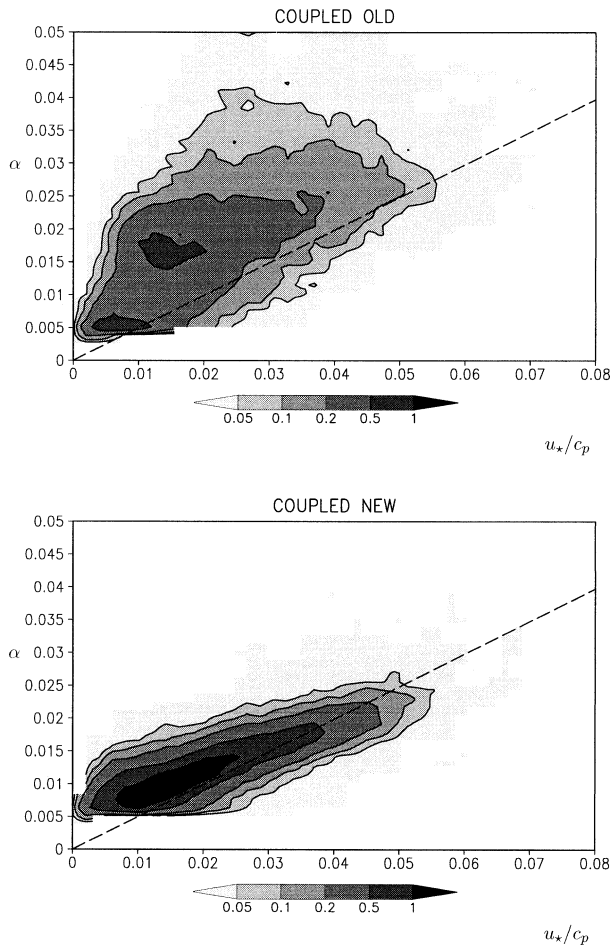
FIG. 5. The Charnock parameter α as a function of inverse wave age u_*/c_p. The Charnock parameters are determined from 6-hourly averaged u_* values and instantaneous u_{10} values. Data of all wind speed classes are gridded and the gray scale gives the fraction of the total number of data points in percentages. (a) The old coupled model. (b) The new coupled model. The dashed line is $\alpha = 0.5\ u_*/c_p$.

First, the median values of the uncorrected Disc2000 data (dashed line) are in good agreement with the bulk parameterization of Smith (1980), who found $C_{d10n} = 0.27 + 0.082$ as the best fit for $u_{10n} > 9$ m s^{-1} (note that the often cited $C_{d10n} = 0.61 + 0.063u_{10n}$ is for the full range of wind speeds). Also the mean ID measurements (open circles) of Hare et al. (1999; Fig. 5) look fairly (but slightly less) similar to those of Smith (1980). However, their mean EC measurements (filled circles) tend to be higher and less biased with respect to the ECMWF model values. The difference between the ID and EC values of Hare et al. (1999) may originate from the differences of the applied flow distortion correction, which in general results in lower Charnock parameters. For the EC method Hare et al. (1999) have corrected only the wind speeds for flow distortion, but not the u_*'s. This may result in a small additional bias in the Charnock parameter.

The three other experiments have clearly higher Char-

TABLE 3. Different bulk parameterizations of the drag coefficient.

Parameterization	Sea-state parameter	Remark
$\alpha = a$	None	Constant Charnock parameter
$C_{d10n} = a + bu_{10n}$	None	Original fit of *Discovery* data
$\alpha = a(\xi)^{-b}$	ξ	Wave-age parameterization

nock parameters. First, three median values (triangles) are estimated from Table 1 of Banner et al. (1999). These values are close to the curve of the ECMWF model, but they are very crude estimates, because the table contains only 29 entries. As a result, the uncertainty in the median values is at least 50%.

The second experiment is that of Eymard et al. (1999), which is represented by the curve of their bulk parameterization. For wind speeds larger (smaller) than 16 m s^{-1}, their Charnock parameter observations are larger (smaller) than those of the ECMWF model. Eymard et al. (1999) and a study of Drennan (2000, personal communication) comparing buoy measurements and measurements during the Flux etat de la mer et Télédétection en Conditions de Fetch Variable (FETCH) experiment suggest that an important reason may be the absence of a flow distortion correction. Such a correction would reduce their Charnock parameters, especially for the strong winds, and therefore enhance the resemblance with the Hare et al. (1999) and Disc2000 data, while reducing it for the ECMWF data. However, according to Drennan (2000, personal communication) the deviations with Smith (1980) are too large to be solely explained by flow distortion. The extent of flow distortion correction in this case should be further investigated. Finally, for the moderate wind cases the Charnock parameters corresponding to the mean neutral drag coefficients of (Zeng et al. 1998, Fig. 1b) are shown. These values are based on the ID measurements in the Tropical Pacific during the TOGA COARE experiment. The Zeng et al. (1998) values are slightly higher than those of the new coupled model, but they are also not corrected for flow distortion and they may have a positive bias due to the stability correction (Taylor and Yelland 2000). In conclusion, the other observational datasets are equivocal with respect to the right magnitude of the Charnock parameter—they all lie between the values given by the Disc2000 and the new version of the coupled ECMWF model.

5. Statistical analyses of different parameterizations

Figure 5 has shown that a wave-age-dependent α is a viable approximation of the drag data of the new coupled model. In this section, we investigate how well the *Discovery* data support a wave-age-dependent parameterization when compared with wind speed only parameterizations. In fact, we make several statistical tests to assess the goodness-of-fit of three parameterizations
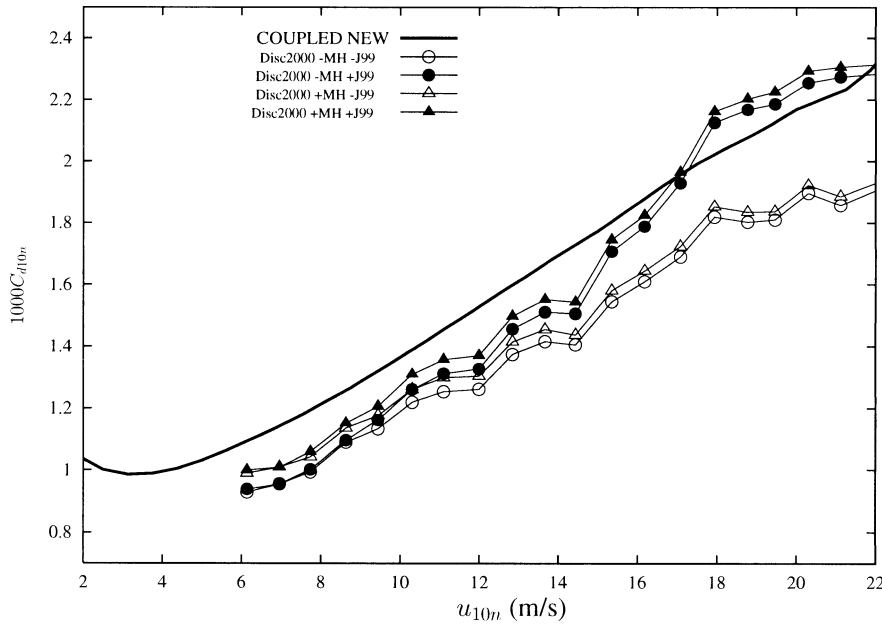
FIG. 6. The mean drag coefficient as a function of wind speed. The thick solid line is for the new coupled model (0147 or ERA40). The thin lines are for the *Discovery* data (Taylor and Yelland 2000). Open (filled) symbols indicate data without (with) the correction of Janssen (1999). The circles (triangles) indicate data without (with) the correction of Donelan (1990).

to the observed data on the basis of the estimates of the random errors discussed in section 3. The three parameterizations are listed in Table 3. In these tests, only *Discovery* data with a wind speed larger than 8 m s^{-1} and with a wind angle within 10° of the bow of the ship are used. The first restriction excludes instances of very dominant swell. The latter selects the data that are corrected for flow distortion by the same simulation of the flow around the ship (Yelland et al. 1998). The restrictions reduce the total number of data to $n = 730$.

The first two parameterizations of Table 3 do not have an explicit parameter of the sea state. The first, the constant Charnock parameter case corresponds to the old version of the ECMWF version, see section 2. The second parameterization is the widely used linear regression with u_{10n}. According to Yelland et al. (1998), this parameterization provides a good description of the observed data, given the random errors. However, as a theoretical parameterization $C_{d10n} = a + bu_{10n}$ is incomplete without a scaling of the b term. This scaling may be sea-state related, but it does not necessarily have to be a wave age. Specifying alternative scalings of the b-term is beyond the scope of paper. Therefore, the linear relation is used in the statistical comparison as it is.

The last parameterization depends on the wave age ξ. Following J99, sea-state information is taken from an uncoupled WAM model run and is collocated on the cruises of the RRS *Discovery*. Several choices for ξ can be made as will be discussed below. The most detailed results are shown for

$$\xi = \frac{c_p}{u_*^{\mathrm{wam}}}, \qquad (19)$$

where u_*^{wam} and c_p are the collocated WAM model friction velocity and peak wave speed, respectively. This ξ estimator is consistent with the modeled wave spectrum and does not depend on the observed friction velocity u_*^{obs}. A disadvantage of this estimator is the hampered representation of high frequent variability due to the 6-hourly update of both u_*^{wam} and c_p.

The parameterizations are fitted to the Disc2000 data using a weighted least squares method. To make a justifiable fit, several aspects with respect to the observational errors and data distribution should be taken into account. First, least squares fitting is based on the Gaussianity of the residuals. This requirement can hardly be fulfilled when modeled α's are fitted to the observed ones, because the distribution of the random errors in the latter are very skewed. Instead, friction velocity approximations from the bulk parameterizations u_*^{par} are fitted to the u_*^{obs} values. For the ($C_{d10n} = a + bu_{10n}$) parameterization, u_*^{par} can be obtained as a function of the observed neutral wind speed u_{10n}^{obs} by

$$u_*^{\mathrm{par}} = (a + bu_{10n}^{\mathrm{obs}})^{1/2} u_{10n}^{\mathrm{obs}}. \qquad (20)$$

For the last parameterizations of Table 3 u_*^{par} is calculated from u_{10n}^{obs} and (ξ) by solving $z_0 = \alpha u_*^2/g$ implicitly for u_*.

Second, the weighting factors of the fit must account for the random errors in the observations and in the

collocated wave age. The most dominant random errors are those of u_*^{obs}. However, also the random errors in u_{10n}^{obs} and ξ play a significant role. To calculate the weight factor, we have assumed an effective relative error $\epsilon_{u*}^{\text{eff}}$ for u_*^{obs}. This error compensates for the random errors in u_*^{obs} and, if applicable, in ξ. The magnitude of $\epsilon_{u*}^{\text{eff}}$ is based on a linear approximation of the random error in C_{d10n} by assuming $\epsilon_{u*}^{\text{eff}} = \epsilon_{C_{d10n}}/2$ [see Eq. (14)]. In fact, $\epsilon_{u*}^{\text{eff}}$ is calculated from

$$(\epsilon_{u*}^{\text{eff}})^2 = \epsilon_{u*}^2 + \epsilon_u^2 + \epsilon_{\text{wave}}^2, \qquad (21)$$

where ϵ_{u*} and ϵ_u are the estimates of Yelland et al. (1994) [see Eqs. (12) and (13)], and ϵ_{wave} the additional random error in u_* due to random errors in ξ. The latter is zero for the first two parameterizations of Table 3, but for the wave-age-dependent parameterization ϵ_{wave} equals to 0.03. This value is derived from Monte Carlo simulations with the wave-age parameterization. In these simulations the representativeness error of c_p is assumed to be Gaussian with a standard deviation of 30%. This deviation is based on the inaccuracy of the WAM c_p approximation ($\approx 10\%$) and the effect of collocating over the WAM model grid and time step (an additional factor 3). Here $\epsilon_{u*}^{\text{eff}}$ equals 6.7% and 7.4% for the wind-speed-only and wave-age-dependent parameterizations, respectively.

Third, as can be seen in Fig. 1 the observations are unequally distributed over different wind speed classes. To avoid a too strong weighting of the moderate wind observations, the observed values are divided over wind speed bins. The reciprocal of the number of observations in the wind speed bin is used as an additional weighting. Hence, the quadratic cost function for the parameterized friction velocity is given by

$$J = \sum_{j=1}^{m} \left[\frac{1}{n_j} \sum_{i=1}^{n_j} \left(\frac{u_*^{ij,\text{obs}} - u_*^{ij,\text{par}}}{\sigma_{u_*}^j} \right)^2 \right],$$
$$\sigma_{u_*}^j = \epsilon_{u*}^{\text{eff}} \overline{u_*^{\text{obs}}}^j, \qquad (22)$$

where ($m = 25$) is the number of wind speed bins and n_j (≥ 8) the number of data in the bin. Here $\overline{u_*^{\text{obs}}}^j$ is the observed friction velocity averaged over the wind speed bin. Optimal values for the constants a and (if present) b are obtained by minimizing J.

In Fig. 8, the error estimate $\sigma_{u_*}^j$ is plotted together with the standard deviation of $u_*^{ij,\text{obs}}$ in the 25 wind speed bins. For moderate values of u_{10n} the scatter in $u_*^{ij,\text{obs}}$ is larger than this error estimate, which suggests that there might be other sources of variability than just the random errors in the observations (e.g., Drennan et al. 1999). For wind speeds over 18 m s^{-1}, $\sigma_{u_*}^j$ is rather large when compared to the standard deviation of scatter. The latter may be somewhat noisy possibly due to the limited number of observations. However, in the case of really accurate EC measurements the error estimate $\sigma_{u_*}^j$ would increase less strongly for the high wind speeds due to the $1/\sqrt{u_{10n}}$ factor in ϵ_{u*} [see Eq. (11)]. Considering this, the $\epsilon_{u*}^{\text{eff}}$ estimate may be some-

what pessimistic for the Disc2000. On the other hand, the ID method may really be less accurate for the high wind speeds when compared to accurate EC measurements. Additional calculations in which ϵ_{u*} was scaled with $1/\sqrt{u_{10n}}$ are made (assuming $\epsilon_{u*} = 0.06$ for $u_{10n} = 10$ m s^{-1}). The results of these calculations are not shown in this paper because, qualitatively, they give the same answers as those discussed below.

To test the goodness-of-fit of the parameterized friction velocity three statistics are considered. The first is a χ^2 statistic for the individual values of u_*. It is given by

$$\chi_p^2 = \sum_{j=1}^{m} \sum_{i=1}^{n_j} \left(\frac{u_*^{ij,\text{obs}} - u_*^{ij,\text{par}}}{\sigma_{u_*}^j} \right)^2. \qquad (23)$$

The χ_p^2 statistic is equal to J except for the weighting factor ($1/n_j$). In addition, a χ^2 statistic for the mean values in the wind speed bins is calculated. This statistic is defined as

$$\chi_b^2 = \sum_{j=1}^{m} n_j \left(\frac{\overline{u_*^{\text{obs}}}^j - \overline{u_*^{\text{par}}}^j}{\sigma_{u_*}^j} \right)^2, \qquad (24)$$

where the averaging within the bin is denoted by the overline. If the error in the friction velocities are indeed Gaussian distributed with standard deviation $\sigma_{u_*}^j$, then χ_b^2 and χ_p^2 should hint upon the same goodness of fit. Finally, a root-mean-square error

$$r = \left[\frac{1}{n} \sum_{j=1}^{m} \sum_{i=1}^{n_j} \left(\frac{u_*^{ij,\text{obs}} - u_*^{ij,\text{par}}}{\overline{u_*^{\text{obs}}}^j} \right)^2 \right]^{1/2} \qquad (25)$$

is calculated to have a measure that is independent of $\epsilon_{u*}^{\text{eff}}$.

The values of J, r, and the χ^2 statistics for the uncorrected Disc2000 data are listed in part I of Table 4. The bulk parameterization with the lowest cost J/n is the wave-age-dependent fit. The second best fit in terms of J/n and r is for the ($C_{d10n} = a + bu_{10n}$) parameterization. Remarkably, the χ_b^2 value is the lowest, despite the low value of $\epsilon_{u*}^{\text{eff}}$. This suggests that the difference in goodness of fit with that of the wave-age parameterization is small. The poorest case by far is the constant α bulk parameterization. The values of J, r, χ_p^2, and χ_b^2 exceed significantly those of the other two.

Owing to the fact that the error estimates are assumed to be normally distributed, the χ_p^2 and χ_b^2 must satisfy a chi-squared distribution as already suggested by their names. These are well known and can be expressed as Gamma distributions (see, e.g., Press et al. 1992) with ($n - k$) and ($m - k$) degrees of freedom, respectively. Here k is the number of optimized constants (either 1 or 2). For both statistics, the probabilities of exceedence, P_p and P_b, are calculated. These are the probabilities that we make an error if we reject the fit given the estimate for the random errors. The largest probability of exceedence is the P_b for the ($C_{d10n} = a + bu_{10n}$). The value is 73%, which suggest that this parameterization is a fairly good description for the mean relation be-
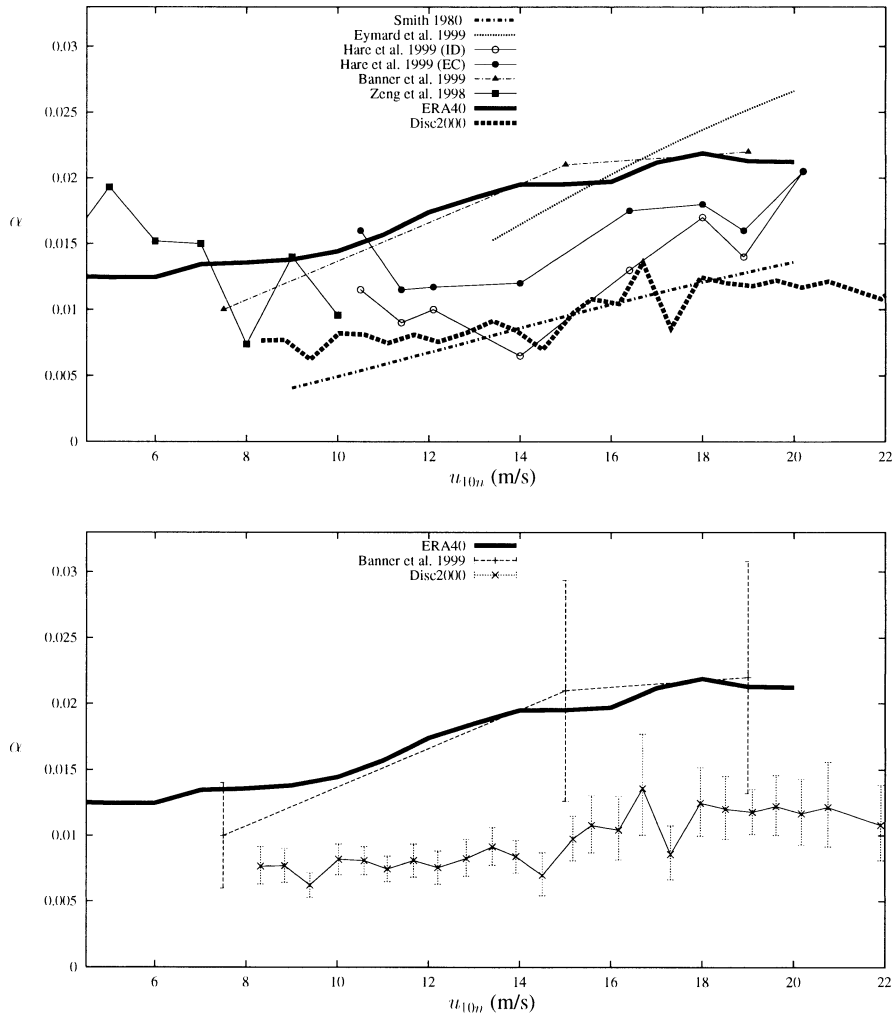
FIG. 7. The Charnock parameter as a function of wind speed. (a) The solid line is the median value for the new coupled model. The dashed line is the median value for the *Discovery* data (Taylor and Yelland 2000). The dashed–dotted (dotted) line is inferred from the bulk formula of Smith (1980) (Eymard et al. 1999). The estimated median observations of Banner et al. (1999) and the mean observations of Hare et al. (1999) are plotted as triangles and circles, respectively. For the latter, the filled (open) circles refer to the eddy correlation (inertial dissipation) method. (b) Indications of the random errors in the median values of Taylor and Yelland (2000) and Banner et al. (1999). The error bars are an approximation of the 90% confidence interval.

tween the wind and wind stress. The second highest value is for the fit of wave-age parameterization ($P_b = 56\%$). All other values of both P_p and P_b are smaller than 0.1%. Therefore, P_p and P_b are not listed in Table 4. To summarize, on the basis of all χ^2 statistics and the assumed error estimates, all three parameterizations must be considered as incomplete descriptions of the uncorrected observed surface drag.

Next, we discuss the combined impact of the measurement height and J99 corrections. The bulk parameterizations of Table 3 are fitted to corrected data in the same manner as has been done for the uncorrected data. The results of the optimal fits and the statistical test are listed in Table 4, with parts II, III, and IV for the MH, the J99, and the combined MH and J99 correction, re-

spectively. When only the height is corrected, all bulk parameterizations have lower values for the cost function and the probabilities of exceedence for the χ^2 statistics are slightly higher. Thus, the height correction improves the goodness of fit. However, whenever the J99 correction is applied the goodness of fit deteriorates considerably. The largest deterioration is observed for the constant Charnock case. The J99 correction enlarges the difference between the surface drag coefficients at the low and high wind speeds (see Fig. 6). Clearly, the single Charnock parameter is not able to account for this effect.

As stated above, an important issue is the approximation of the wave age. A drawback of c_p/u_*^{wam} is its reduced representation of high frequent variability due
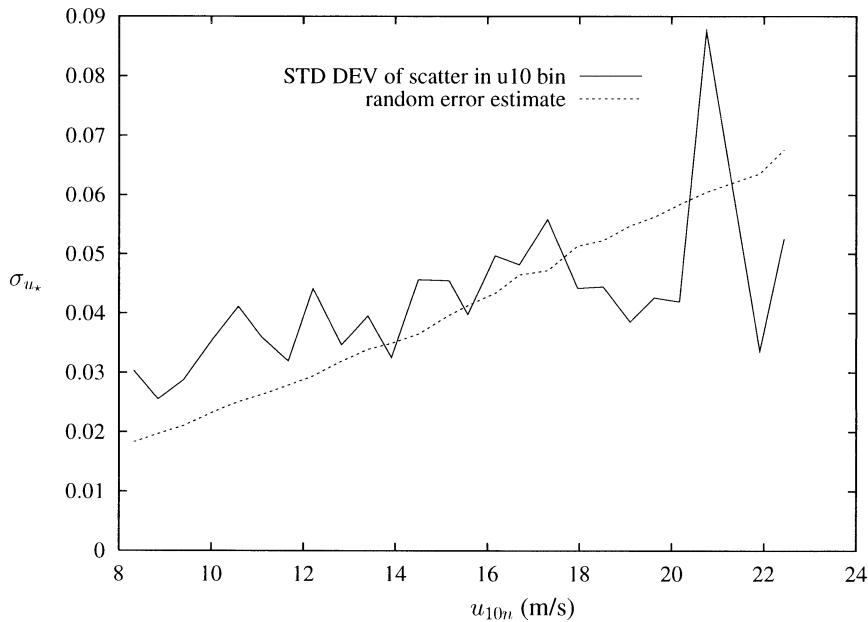
FIG. 8. Standard deviation of the scatter of observed u_*'s in subsequent wind speed bins of approximately 0.5 m s^{-1} (solid line). In addition, the error estimate $\sigma_{u_*} = \epsilon_{u*}^{\mathrm{eff}} u^{\mathrm{obs}}$ [(see Eq. 24)] in these wind speed bins (dotted line) is shown. The value of $\epsilon_{u*}^{\mathrm{eff}}$ (6.7%) is for the wind-speed-only parameterizations.

to the WAM time step of 6 h. To explore the impact of this choice, calculations with three reasonable alternatives are made. Table 5 lists the results of the alternative wave-age bulk parameterizations for the uncorrected Disc2000 data. The first approximation, $c_p/u_{10n}^{\mathrm{wam}}$ is also consistent with the model wave spectrum and the fit to the observed data is only slightly worse. The best results for the individual observations are obtained with c_p/u_*^{obs}. However, a complication with this approximation

is that u_* is used both as an endogenous and exogenous variable. This double role of u_*^{obs} spuriously enhances the goodness of fit of the bulk parameterization. On the other hand, an argument for using this wave age is that it might be the best representation of the wave-age variability given the available data. This parameterization is still an incomplete description of the observed variability in the surface drag, because $\chi_p^2/(n-k) = 1.04$ gives a P_p of 23%, which is a too small probability of

TABLE 4. Optimal parameters and χ^2 statistics for different parameterizations. Part I is for the uncorrected Disc2000 data. In part II to IV, the MH, J99, and the combined MH and J99 corrections are applied, respectively.

Parameterization	a	b	J/n	r	$\dfrac{\chi_p^2}{n-k}$	$\dfrac{\chi_b^2}{m-k}$
Part I		$-$MH $-$ J99				
$\alpha = a$	0.00985	—	0.0485	0.0865	1.66	5.78
$C_d = a + bu$	0.501	0.0675	0.0436	0.0821	1.50	0.80
$\alpha = a(u_*^{\mathrm{wam}}/c_p)^b$	0.0816	0.681	0.0346	0.0809	1.21	0.93
Part II		$+$MH $-$ J99				
$\alpha = a$	0.0109	—	0.0454	0.0836	1.56	3.76
$C_d = a + bu$	0.564	0.0657	0.0424	0.0810	1.46	0.82
$\alpha = a(u_*^{\mathrm{wam}}/c_p)^b$	0.0809	0.646	0.0338	0.0798	1.18	0.93
Part III		$-$MH $+$ J99				
$\alpha = a$	0.0147	—	0.0703	0.102	2.29	20.66
$C_d = a + bu$	0.232	0.0971	0.0507	0.0869	1.68	2.03
$\alpha = a(u_*^{\mathrm{wam}}/c_p)^b$	0.278	0.948	0.0443	0.0885	1.46	3.77
Part IV		$+$MH $+$ J99				
$\alpha = a$	0.0162	—	0.0650	0.0975	2.11	16.44
$C_d = a + bu$	0.291	0.0958	0.0497	0.0858	1.64	2.07
$\alpha = a(u_*^{\mathrm{wam}}/c_p)^b$	0.222	0.844	0.0424	0.0864	1.39	3.21

TABLE 5. Optimal parameters and χ^2 statistics for different wave-age parameterizations.

Parameterization	a	b	J/n	r	χ_p^2 $n - k$	χ_b^2 $m - k$
$\alpha = a(u_{10n}^{\text{wam}}/c_p)^b$	0.00987	0.832	0.0349	0.0811	1.22	1.17
$\alpha = a(u_*^{\text{obs}}/c_p)^b$	0.227	0.983	0.0305	0.0748	1.04	1.34
$\alpha = a(utenn^{\text{obs}}/c_p)^b$	0.00957	0.707	0.0375	0.0829	1.28	1.65

exceedence. The worst results are obtained with the last wave age, c_p/u_{10n}^{obs}. In this case the r value is slightly lower than that of the $(C_{d10n} = a + bu_{10n})$ bulk parameterization, despite the extra variability due to u_{10n}. Similar results are obtained for the corrected Disc2000 data. In short, the effects of different wave-age approximations on the goodness of fit of the wave-age bulk parameterization are considerable, but for the qualitative comparison with the other bulk parameterization the impact is small.

The comparable quality of the $C_{d10n} = a + bu_{10n}$ and the $\alpha = a(u_*^{\text{wam}}/c_p)^b$ parameterizations is depicted in Figs. 9 and 10. In Fig. 9, C_{d10n} is plotted as a function of u_{10n}. Clearly, the increase of the C_{d10n} with u_{10n} of the wave-age parameterization is practically equal to the slope of the $(C_{d10n} = a + bu_{10n})$. In addition, for fixed wind speeds it has slightly more variability. However, the magnitude of this variability combined with the estimated observational errors is still insufficient to explain the total scatter in the wind speed bins as is demonstrated by the χ^2 statistics. In Fig. 10, $\ln(\alpha)$ is plotted as a function of the WAM inverse wave age. As a result of the observational errors, many $\log(\alpha)$ observations

are much smaller than the optimal fits (see section 3). Both fits depict an increase of α with the inverse wave age, but for the $C_{d10n} = a + bu_{10n}$ parameterization the increase with the inverse wave age is smaller. This lower increase results in rather low α's for wave ages smaller than 20 and high α's for wave ages higher than 30.

To further explore the difference between the $C_{d10n} = a + bu_{10n}$ and the $\alpha = a(u_*^{\text{wam}}/c_p)^b$ parameterization, the distributions of the residuals in wind stress ($\tau^{\text{obs}} - \tau^{\text{par}}$) are analyzed. These analyses are made for different wave-age classes. The distribution of the residuals is compared with a modeled "error" distribution. The modeled error distribution is generated by a Monte Carlo simulation of the wind stress residuals that are solely due to the random errors in the observed u_* (6%), u_{10n} (3%), and (if applicable) the modeled wave age (u_*^{wam}/c_p) (30%). For these values of the relative errors, the error distribution of residuals are dominated by the errors in u_*. In Fig. 11, the distributions are plotted for the classes of old waves (top panels), waves with an intermediate age (middle panels), and young waves (bottom panels). For both bulk parameterization, the differences between the observed and estimated error
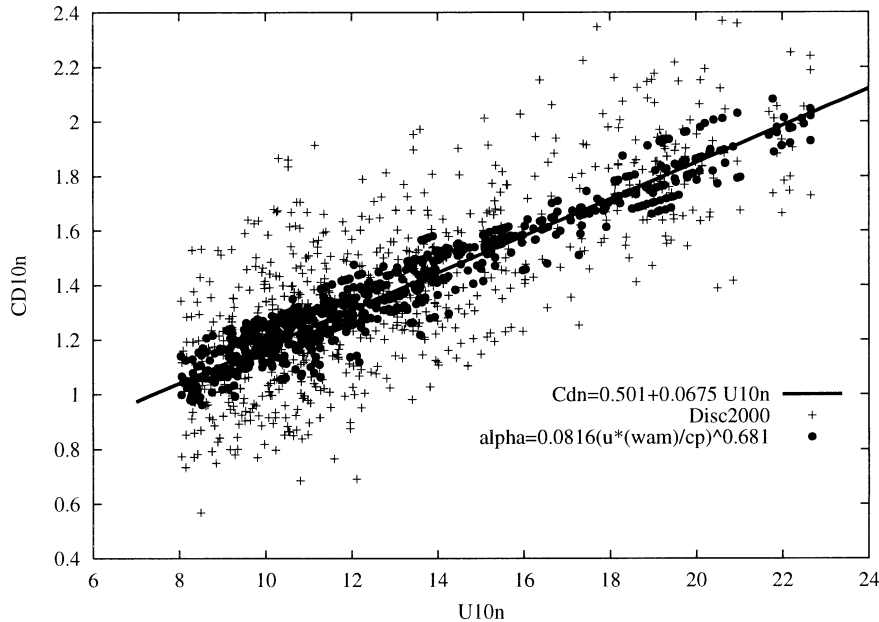
FIG. 9. The neutral drag coefficient C_{d10n} as a function of neutral wind speed u_{10n}. The observations are plotted as crosses. The bulk parameterization $C_{d10n} = 0.501 + 0.0675u_{10n}$ is plotted as a solid line. The values of C_{d10n} calculated with the observed u_{10n} and the $[\alpha = a(u_*^{\text{wam}}/c_p)^b]$ parameterization where $a = 0.0816$ and $b = 0.681$ are plotted as filled circles.
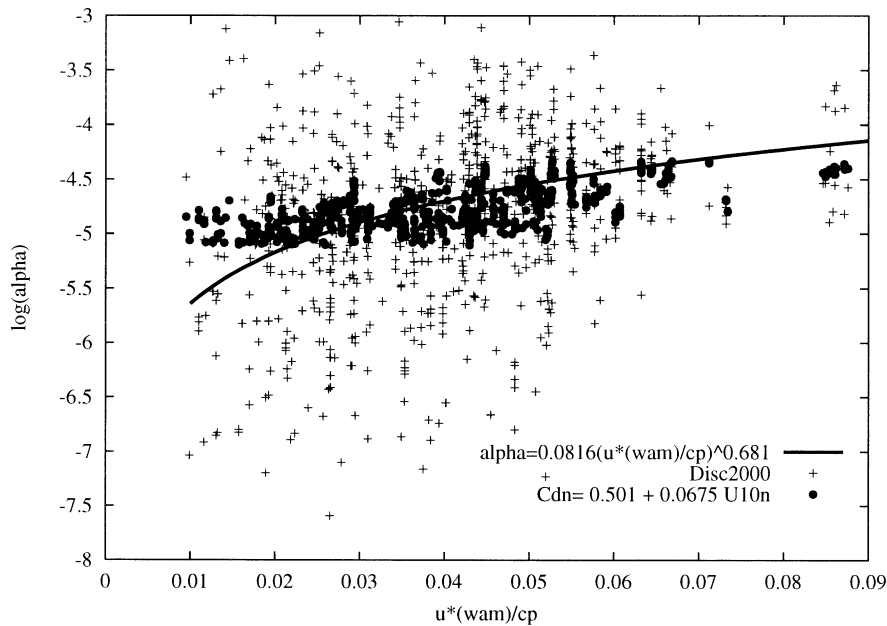
Fig. 10. The Charnock parameter α as a function of the inverse wave age u_*^{wam}/c_p. The [$\alpha = a(u_*^{wam}/c_p)^b$] parameterization, with $a = 0.0816$ and $b = 0.681$ is plotted as as a solid line. The observations are plotted as crosses. Values from the bulk parameterization $C_{d10n} = 0.501 + 0.0675u_{10n}$ are plotted as filled circles.

distributions are not dramatic for the classes of old waves and waves with an intermediate age. However, for young waves the ($C_{d10n} = a + bu_{10n}$) parameterization demonstrates an underestimation of the observed stresses. This underestimation is not observed for the $\alpha = a(u_*^{wam}/c_p)^b$ parameterization. The similarity of the error and residual distributions are quantified by means of the Kuiper statistic (e.g., Press et al. 1992, p. 621). This is a nonparametric statistical test based on the maximum positive and maximum negative difference (V_{kp}) in the cumulative distributions. The probabilities of exceedence (P_{kp}) are calculated from the associated probability density function. The Kuiper values V_{kp} and the probabilities P_{kp} are displayed at the top of the panels. The Kuiper statistics give in general low probabilities of exceedence. These low values confirm that the bulk parameterizations are an incomplete representation of the observed data given the estimates of the relative errors. However, for the young wave class the P_{kp} value of the $C_{d10n} = a + bu_{10n}$ parameterization (0%) is considerably smaller than that of the $\alpha = a(u_*^{wam}/c_p)^b$ parameterization (7%). This suggests that the latter bulk parameterization provides a better representation of the observed wind stress for the class of young waves. However, the value of P_{kp} (7%) is not large enough to accept the wave-age parameterization with a large (e.g., 10%) significance level.

6. Discussion and conclusions

As depicted in Figs. 4 and 7, there is some controversy about the magnitude of the Charnock parameter and

hence the drag coefficient. The controversy is most vivid in the comparison of, on the one side, the new ECMWF model ($C_{d10n} \approx 0.00135$ for $u_{10n} = 10$ m s^{-1}), and, on the other side, the observations of Taylor and Yelland (2000) ($C_{d10n} \approx 0.00115$ for $u_{10n} = 10$ m s^{-1}). First we discuss the observations.

One may assume the position that the open ocean drag coefficients of Taylor and Yelland (2000) are too low. Comparisons with some other open ocean experiments (see Fig. 7) hint upon this view. These experiments are TOGA COARE (Fairall et al. 1996) for the moderate wind speeds, SOWEX (Banner et al. 1999) and FASTEX, that is, the eddy correlation of Hare et al. (1999) and the ID measurements of Eymard et al. (1999). Other careful wind stress measurements find even higher drag coefficients. A good example is the Humidity Exchange over the Sea (HEXOS) experiment (Smith et al. 1992). However, there is still a lot of ongoing discussion about the quality of these measurements and their interpretation of systematic errors. For example, Eymard et al. (1999) did not apply a correction for flow distortion by the ship. In the case of Banner et al. (1999), the number of observations are too small to make firm statements. The HEXOS experiment was made in a coastal area. It is still a matter of research under which conditions these observations may be representative for the open ocean. Therefore, one should be reluctant in drawing conclusions from elementary comparisons.

Following the assumption that the Disc2000 drag data are too low, two corrections have been considered in
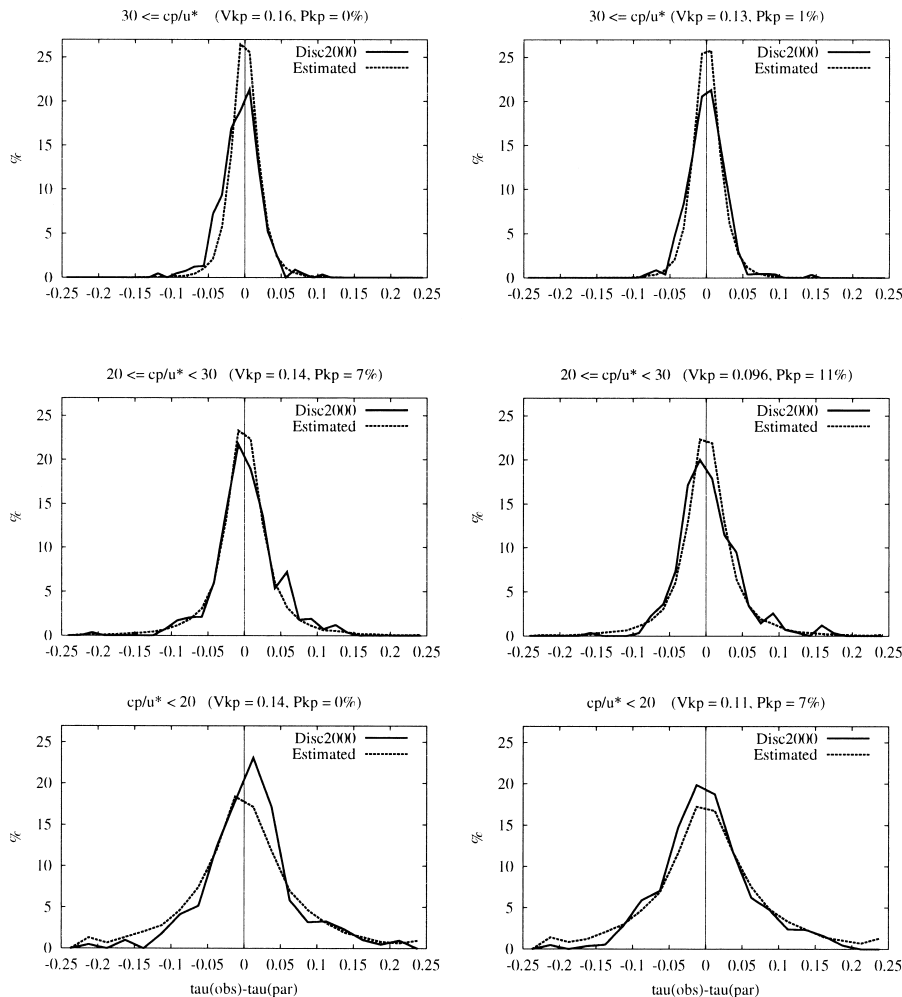
FIG. 11. Histograms of the wind stress differences $\tau^{obs} - \tau^{par}$ (solid line) for the three wave-age classes. These classes are (top panels) mature, (middle panels) intermediate, and (bottom panels) young. The left (right) panels are for the $C_{d10n} = a + bu_{10n}$ [$\alpha = a(u_*^{wam}/c_p)^b$] bulk parameterization. The theoretical distribution on the basis of the relative errors in u_*^{obs}, u_{10n}^{obs}, and (if applicable) c_p/u_*^{wam} are indicated by the dashed lines. Probabilities of exceedence based on the Kuiper statistic for the differences in the distribution are denoted at the top of the panels.

this paper to enhance them. These are the correction for the measurement height (MH) and for the neglect of fluctuations in the TKE balance caused by the surface waves (J99). Both corrections are unable to solve the controversy. First, the MH correction is of the right sign to reduce the discrepancy with, for example, the new coupled model. In addition, it gives a correction for all wind speed ranges and the goodness of fit of the bulk parameterizations to the observed data increases (Table 4). However, the correction is by far too small to explain the magnitude of the bias. Second, the J99 correction has the right sign and magnitude, but only for the strong winds. In addition the J99 increased the lack of fit of widely used bulk parameterizations. The magnitude of the J99 correction is still under discussion (Taylor and Yelland 2001; Janssen 2001).

The alternative point of view is that the mean values

of Disc2000 are of the right magnitude. The Disc2000 dataset is by far the longest record, which implies that many different geophysical conditions are sampled by a reasonable number of observations. In addition, Yelland et al. (1998), Henjes et al. (1999), and Taylor and Yelland (2000) have made a careful study of the flow distortion problem and possible shortcomings of their ID method. Other cruises with the same setup confirm the Disc2000 magnitude of the stress. Strongest support from a different source are the EC measurements of Smith (1980), because they are made from a well-exposed anemometer. Also the ID measurements of Hare et al. (1999) are in the range of the Disc2000 data.

We now come to the model data. In section 4, the mean surface-drag coefficients of different versions of ECMWF's coupled atmosphere–wave model were tested against those from the uncoupled model and those from

observations. For all wind speed ranges, the old coupled model has a positive bias with respect to the uncoupled model ($\alpha = 0.018$). However, the mean drag coefficients resulting from the new coupled model (ERA40) version are on average nearly equal to those of the uncoupled (ERA15) version. The drag coefficient of the new coupled version is slightly smaller (larger) for wind speeds smaller (larger) than 12 m s^{-1}, which results in better agreement with the slope of the Disc2000 C_{d10n}–u_{10n} relation (see Fig. 4). When compared with the Disc2000 observations, all model drag coefficients have a significant positive bias for all wind speeds. However, with TOGA COARE, SOWEX, and the results of Eymard et al. (1999) the new coupled model has a fair agreement.

Next, we discuss the results of statistical analyses of the different bulk parameterizations. To make justifiable fits to the data, an approximation of the random observation error in u_* as function of u_{10n} was derived on the basis of published estimates of these errors (e.g., Yelland et al. 1994; Sreenivasan et al. 1978). According to the derived estimate ($\epsilon_{u*}^{\mathrm{eff}}$) not all of the scatter in wind stress for a fixed wind speed can be attributed to the random observational errors in u_* and u_{10n} (see Fig. 8). Consequently, it is conceivable that a third (geophysical) parameter explains the surplus of variance. Sea-state parameters are good candidates and therefore the wave age is checked by statistical tests.

First, the positive bias of the ECMWF model when compared with the Disc2000 data is confirmed by the computed constants of the bulk parameterization in section 5. For example, in the constant Charnock case for the uncorrected Disc2000 data, α equals 0.010 rather than 0.018, which is used in the uncoupled model.

Second, from the statistics of the optimal fits of the bulk parameterizations to the corrected and uncorrected open ocean measurements it is concluded that all the considered bulk parameterizations can be statistically rejected as sufficiently complete descriptions of the surface drag given the estimate of the random errors in the observed data.

The largest lack of fit is obtained for the constant Charnock parameter case. This fact confirms the conclusion of Yelland et al. (1998) that this bulk parameterization is inferior to describe the *Discovery* data. In addition, a similar result was found by (Janssen 1997) for the HEXOS data.

Third, with respect to wind speed bin-averaged wind stresses, the wave-age-dependent and $C_{d10n} = a + bu_{10n}$ bulk parameterization perform equally well to the goodness-of-fit test. However, the first parameterization scores slightly better on the tests for the individual points. This difference suggests a small preference for a wave-age-dependent bulk parameterization, because it hints upon an improved description of the geophysical variance.

As a final remark, we note that all bulk parameterizations considered in this paper had to be rejected as fully explaining the observed variance. This may hint at some interesting underlying physics, but it could also be due to the choice of the bulk parameterization, or to our use of modeled wave data (for lack of direct observations) or shortcomings in the error estimates. To fully resolve these issues further research is needed as was also noted recently by the WCRP/SCOR working group on air–sea fluxes (WGASF 2000, chapter 12). We hope that the discussions in this paper will contribute to the preparation of future experiments, which would, in our opinion, only make sense if they involve long records of high quality measurements for a broad range of *experimentally resolved* geophysical conditions. The adequate assessment of observational errors will continue to be important.

REFERENCES

Banner, M., W. Chen, E. Walsh, J. Jensen, S. Lee, and C. Fandry, 1999: The Southern Ocean Wave Experiment. Part I: Overview and mean results. *J. Phys. Oceanogr.,* **29,** 2130–2144.

Bidlot, J., B. Hansen, and P. Janssen, 1999: Ocean waves project memorandum. ECMWF Research Department Memo. R60-G, 15 pp.

Charnock, H., 1955: Wind stress on a water surface. *Quart. J. Roy. Meteor. Soc.,* **81,** 639–640.

Donelan, M., 1990: Air–sea interaction. *The Sea.* Vol. 9: *Ocean Engineering Science,* B. Le Mehaute and D. M. Hanes, Eds., Wiley and Sons, 239–292.

Drennan, W., H. C. Graber, and M. A. Donelan, 1999: Evidence for the effects of swell and unsteady winds on marine wind stress. *J. Phys. Oceanogr.,* **29,** 1853–1864.

ECMWF, 1998: Physical processes. ECMWF Integrated Forecasting System Tech. Documentation 4, 146 pp.

Eymard, L., and Coauthors, 1999: Surface fluxes in the North Atlantic Current during CATCH/FASTEX. *Quart. J. Roy. Meteor. Soc.,* **125,** 3562–3599.

Fairall, C., E. Bradey, D. Rogers, J. Edson, and G. Young, 1996: Bulk parameterization of air–sea fluxes for the Tropical Ocean Global Atmosphere Coupled Ocean–Atmosphere Response Experiment. *J. Geophys. Res.,* **101,** 3747–3764.

Garrat, J., 1992: *The Atmospheric Boundary Layer.* Cambridge Atmospheric and Space Science Series, Cambridge University Press, 316 pp.

Gibson, R., P. Kållberg, S. Uppala, A. Hernandez, A. Nomura, and E. Serrano, 1997: The ERA description. The ECMWF Re-Analysis Project Report Series 1, 74 pp.

Hare, J., P. Persson, C. Fairall, and J. Edson, 1999: Behavior of Charnock's relation for high wind conditions. Preprints, *13th Symp. on Boundary Layers and Turbulence,* Dallas, TX, Amer. Meteor. Soc., 252–255.

Henjes, K., M. Yelland, and P. Taylor, 1999: Effect of pulse averaging on sonic anemometer spectra. *J. Atmos. Oceanic Technol.,* **16,** 181–184.

Janssen, J., 1997: Does wind stress depend on sea state or not? A statistic error analysis of HEXMAX data. *Bound.-Layer Meteor.,* **83,** 479–503.

——, 1989: Wave-induced stress and the drag of air flow over sea waves. *J. Phys. Oceanogr.,* **19,** 745–754.

——, 1991: Quasi-linear theory of wind–wave generation applied to wave forecasting. *J. Phys. Oceanogr.,* **21,** 1631–1642.

——, 1999: On the effect of ocean waves on the kinetic energy balance and consequences for the inertial dissipation technique. *J. Phys. Oceanogr.,* **29,** 530–534.

——, 2001: Ocean waves do affect the kinetic energy balance. *J. Phys. Oceanogr.,* **31,** 2537–2544.

——, and P. Viterbo, 1996: Ocean waves and the atmospheric climate. *J. Climate,* **9,** 1269–1287.

——, J. Doyle, J. Bidlot, B. Hansen, L. Isaksen, and P. Viterbo, 1999: The impact of ocean waves on the atmosphere. *Proc. Seminar on Atmosphere–Surface Interaction,* Reading, United Kingdom, ECMWF, 85–112.

Komen, G., L. Cavaleri, M. Donelan, K. Hasselmann, S. Hasselmann, and J. Janssen, 1994: *Dynamics and Modelling of Ocean Waves.* Cambridge University Press, 532 pp.

——, P. Janssen, V. Makin, and W. Oost, 1998: On the sea state dependence of the Charnock parameter. *Global Atmos. Ocean Syst.,* **5,** 367–388.

Monin, A., and A. M. Obukhov, 1954: Basic laws of turbulent mixing in the ground layer of the atmosphere. *Akad. Nauk. SSSR Geofiz. Inst. Tr.,* **24,** 163–187.

Pierson, W., and L. Moskowitz, 1964: A proposed spectral form for fully developed wind seas based on the similarity theory of S. A. Kitaigorodskii. *J. Geophys. Res.,* **69,** 163–187.

Press, W., S. A. Teukolsky, W. Vetterling, and B. Flannery, 1992: *Numerical Recipes, the Art of Scientific Computing.* Cambridge University Press, 1020 pp.

Smith, S., 1980: Wind stress and heat flux over the ocean in gale force winds. *J. Phys. Oceanogr.,* **10,** 709–726.

——, 1988: Coefficients for sea surface wind stress, heat flux, and wind profiles as a function of wind speed and temperature. *J. Geophys. Res.,* **93,** 15 467–15 472.

——, and Coauthors, 1992: Sea surface wind stress and drag coefficients: The HEXOS results. *Bound.-Layer Meteor.,* **68,** 109–142.

Sreenivasan, K., A. Chambers, and R. Antonia, 1978: Accuracy of moments of velocity and scalar fluctuations in the atmospheric surface layer. *Bound.-Layer Meteor.,* **14,** 341–359.

Sterl, A., and H. Bonekamp, 2000: Comparison of wind stress from ERA and from WAM. *Proc. Second Int. Conf. on Reanalyses,* Reading, United Kingdom, World Meteorological Organisation, 149–152.

——, G. Komen, and P. Cotton, 1998: 15 years of global wave hindcasts using ERA winds. *J. Geophys. Res.,* **103C,** 5477–5492.

Stull, R., 1988: *An Introduction to Boundary Layer Theory.* Atmospheric Science Library, Kluwer Academic Publishers, 670 pp.

Taylor, P., and M. Yelland, 2000: On the apparent ''imbalance'' term in the turbulent kinetic energy budget. *J. Atmos. Oceanic Technol.,* **17,** 82–89.

——, and ——, 2001: Comments on ''On the effect ocean waves on the kinetic energy balance and consequences for the inertial dissipation technique.'' *J. Phys. Oceanogr.,* **31,** 2532–2536.

Uppala, S., J. Gibson, M. Fiorino, A. Hernandez, P. Kållberg, X. Li, K. Onogi, and S. Saarinen, 2000: ECMWF's second generation reanalysis ERA40. *Proc. Second Int. Conf. on Reanalyses,* Reading, UK, United Kingdom, World Meteorological Organisation WMO/TD-No. 985, 9–12.

WGASF, 2000: Intercomparison and validation of ocean–atmosphere energy flux fields. Final report of Joint WCRP/SCOR Working Group on Air–Sea Fluxes (SCOR working group 110). WCRP Rep. 112, WMO/TD-No. 1036.

Yelland, M., 1997: Wind stress over the open ocean. Ph.D. thesis, University of Southampton, 168 pp.

——, and ——, 1999: Does the wind stress depend on the sea-state? *Wind-over-Wave Couplings: Perspectives and Prospects,* S. Sajjadi, N. Thomas, and J. Hunt, Eds., Clarendon Press, 107–118.

——, and P. Taylor, 1996: Wind stress measurements from the open ocean. *J. Phys. Oceanogr.,* **26,** 541–558.

——, ——, I. E. Consterdine, and M. H. Smith, 1994: The use of the inertial dissipation technique for shipboard wind stress determination. *J. Atmos. Oceanic Technol.,* **11,** 1093–1108.

——, B. Moat, P. Taylor, R. Pascal, J. Hutchings, and V. Cornell, 1998: Wind stress measurements from the open ocean corrected for air-flow distortion by the ship. *J. Phys. Oceanogr.,* **28,** 1511–1526.

Zeng, X., M. Zhao, and R. Dickinson, 1998: Intercomparison of bulk aerodynamic algorithms for the computation of sea surface fluxes using TOGA COARE and TAO data. *J. Climate,* **11,** 2628–2644.